Cite this article
Diao M, Li Y, Guan H *et al.*
Post-punching mechanisms of slab–column joints under upward and downward punching actions.
Magazine of Concrete Research,
https://doi.org/10.1680/jmacr.19.00217

Research Article
Paper 1900217
Received 25/04/2019; Revised 21/07/2019;
Accepted 16/09/2019

Keywords: finite element methods/slabs & plates/testing, structural elements

Magazine of Concrete Research

ice Publishing

Post-punching mechanisms of slab–column joints under upward and downward punching actions

Mengzhu Diao
Former Master's student, Key Laboratory of Urban Security and Disaster Engineering of Ministry of Education, Beijing University of Technology, Beijing, China; PhD candidate, School of Engineering and Built Environment, Griffith University Gold Coast Campus, Australia

Yi Li
Associate Professor, Key Laboratory of Urban Security and Disaster Engineering of Ministry of Education, Beijing University of Technology, Beijing, China (corresponding author: yili@bjut.edu.cn)

Hong Guan
Professor, School of Engineering and Built Environment, Griffith University Gold Coast Campus, Australia

Xinzheng Lu
Professor, Key Laboratory of Civil Engineering Safety and Durability of Ministry of Education, Tsinghua University, Beijing, China

Huizhong Xue
PhD candidate, School of Engineering and Built Environment, Griffith University Gold Coast Campus, Australia

Zongda Hao
Master's student, Key Laboratory of Urban Security and Disaster Engineering of Ministry of Education, Beijing University of Technology, Beijing, China

Progressive collapse of reinforced concrete flat plate systems can be significantly influenced by the post-punching performance of their slab–column joints under large deformations. This work presents a series of static collapse tests on four flat slab–column joint specimens with slab in-plane restraint. The effects of different punching directions (upward and downward) and embedded beams on the post-punching performance of the joints were studied. The test results reveal that the post-punching load-bearing and deformation capacities are mainly governed by the longitudinal through-column reinforcement in the slab. The peak bearing capacities and failure modes of specimens without embedded beams were significantly influenced by different punching directions. Conversely, the post-punching mechanisms of specimens with embedded beams were identical regardless of their opposite punching shear actions. In addition, the inclusion of the embedded beams increased the resistance capacity of the specimens under both flexural and suspension mechanisms and enhanced the deformation capacity under the suspension mechanism. Furthermore, a finite-element numerical model was developed and verified against the test results. Based on the numerical study, the contributions of the concrete and reinforcement in resisting the collapse of the slab–column joints were evaluated.

Notation

b	column width
d	width of zone
E	elastic modulus
e	ratio of elongation
F	applied load (kN)
F_{p}	applied load corresponding to punching shear failure (kN)
F_{s}	applied load corresponding to rupture of all through-column rebars (kN)
F_{si} ($i = 1, 2, 3$)	applied loads corresponding to different suspension substages (kN)
F_{t}	applied load corresponding to load mechanism transition (kN)
f_{c}	cubic compressive strength of concrete
f_{u}	ultimate strength
f_{y}	yield strength
h	slab thickness
K	stiffness of load–displacement curve (kN/mm)
L	two-bay span length
L_{s}	length of steel bars
V_{p}	punching shear capacity (kN)
$V_{\mathrm{p,e}}$	experimental punching shear capacity (kN)
$V_{\mathrm{p,s}}$	simulated punching shear capacity (kN)
V_{pp}	post-punching shear capacity (kN)
$V_{\mathrm{pp,e}}$	experimental post-punching shear capacity (kN)
$V_{\mathrm{pp,s}}$	simulated post-punching shear capacity (kN)
α	bend-down angle of top rebars in specimens UPS-1 and DPS-1 (°)
β	bend-down angle of bottom rebars in specimens UPS-1 and DPS-1 (°)
Δ	vertical displacement measured at bottom column stub (mm)
Δ_{e}	vertical displacement corresponding to the end of the test (mm)
Δ_{p}	vertical displacement corresponding to punching shear failure (mm)
Δ_{s}	vertical displacement corresponding to rupture of all through-column rebars (mm)
Δ_{si} ($i = 1, 2, 3$)	vertical displacement corresponding to different suspension substages (mm)
Δ_{t}	vertical displacement corresponding to load mechanism transition (mm)
ε	strain

Introduction

Progressive collapse is defined as the spread of an initial local failure from elements to elements, which eventually results in the collapse of an entire structure or disproportionately large part of it (ASCE, 2010). Over the past few decades, multiple progressive collapse events of reinforced concrete (RC) flat plate structures have occurred worldwide, initiated by punching shear failure at slab–column joints, which is propagated to the rest of the structural system. The catastrophic collapse of Sampoong Department store in South Korea (Gardner *et al.*, 2002), Pipers Row Car Park in the UK (Wood, 2003) and the Gretzenbach underground parking garage in Switzerland (Ruiz *et al.*, 2010) are typical cases of progressive collapse of RC flat plate structures. In recent years, numerous collapse cases of underground car parks in China were also reported. These collapse cases were mostly triggered by punching shear failure at the slab–column joints due to excessive vehicular loading or uneven excavation and dumping of the excavated soil during construction. Brittle punching shear failure is an inherent damage mode of slab–column joints, and cannot be prevented by simply enlarging the sections of structural elements or increasing the reinforcement ratio. Conversely, if the slab–column joints are properly designed, a considerable amount of collapse resistance by the so-called suspension mechanism after the punching failure can be provided. Given that progressive collapse is an event with low probability, adequate post-punching strength and deformation capacity are considered an effective and low-cost secondary defence for preventing the propagation of progressive collapse. Therefore, it is important to investigate the post-punching mechanism and resistance of the slab–column joints to mitigate the progressive collapse of flat plate systems.

A series of experimental tests was conducted to investigate the post-punching mechanisms of flat slab–column joints, in which three key aspects were specially considered in the specimen design and loading pattern: (*i*) different punching directions; (*ii*) slab in-plane restraint; (*iii*) strengthening technique – that is, embedded beams. These aspects are described next with reference to the relevant literature.

Different punching directions

There are two types of punching shear failure modes of slab–column joints in a flat plate structure, as shown in Figure 1: (*i*) upward punching shear (UPS) failure, showing an inverted conical damage pattern, which is caused by overloading of the slab directly or indirectly through redistribution of the internal forces of the slab during the process of collapse; (*ii*) downward punching shear (DPS) failure, in the form of a cone, which is usually triggered by an uplifting action to the slabs, and is probably generated from a blast or hydrodynamic forces induced by a hurricane (Dusenberry, 2010; Robertson *et al.*, 2007). Note that either a DPS or a UPS failure might trigger progressive collapse. In addition, progressive collapse is a complicated mechanical process of structural systems, in which subsequent UPS and DPS damages can occur at the adjacent slab–column joints, owing to the redistributed loads acting on the slabs and columns, respectively. Currently, most studies have centred on the punching shear behaviour of slab–column joints under the UPS mode of failure (Carvalho *et al.*, 2011; Ruiz *et al.*, 2010). Various parametric studies have been conducted to explore the influence of such factors as the concrete strength, reinforcement ratio, size of column, reinforcement layout, size effect and shear reinforcement on the punching shear strength and failure behaviour of flat slab structures (Criswell, 1974; Elstner and Hognestad, 1956; Guandalini *et al.*, 2009). However, to the authors' knowledge, no study of the DPS failure mode has been reported to date.

Slab in-plane restraint

In a real flat plate structure, the slab–column joints are in-plane constrained by surrounding slabs. Such a constraint allows the joints to exhibit a suspension mechanism after punching shear failure occurs, thereby providing load redistribution resistance through large tensile forces developed in the reinforcing bars. Experimenters have investigated the

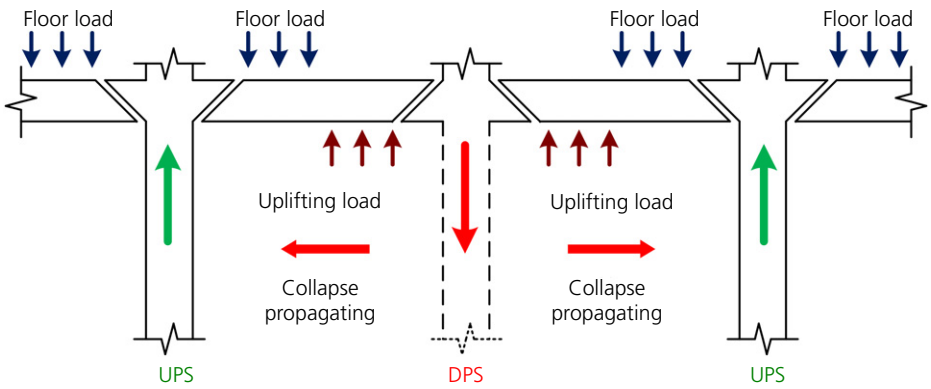

Figure 1. Failure modes of slab–column joints in progressive collapse

post-punching mechanisms, including damage to the compressive zone around the columns (Mirzaei, 2010), the contribution of the integrity reinforcement (IR) (Hawkins and Mitchell, 1979; Melo and Regan, 1998; Mirzaei, 2010), the tensile membrane action (McPeake, 1980) and the effects of structural parameters on the post-punching behaviour (Habibi *et al.*, 2012). Despite these research efforts, almost all of the aforementioned slab–column joint test specimens were extracted from a prototype structure approximately along the lines of contraflexure and were simply supported along their edges; the in-plane restraint from the surrounding slabs was neglected (Liu, 2014). Only a limited number of slab–column joint tests have accounted for the effect of the slab in-plane restraint (Keyvani *et al.*, 2014; Mitchell and Cook, 1984; Peng *et al.*, 2017). Mitchell and Cook (1984) reported that well-anchored through-column IR is capable of connecting the punching cone to the slab, holding the slab from falling down and enabling load transfer from the column stud to the slab. The enhancement of the in-plane restraint on the punching shear strength was evaluated by Keyvani *et al.* (2014), who found that the punching shear strength increased by 17% and 34%, respectively, in an actual flat plate structure and in a fully restrained isolated joint, owing to the compressive membrane action. Peng *et al.* (2017) concluded that sufficient lateral restraint provided by the slab boundary could increase the punching capacity of slab–column joints and their post-cracking flexural stiffness. Given the lack of study on the influence of the slab in-plane restraint provided by the surrounding structure on the behaviour of isolated slab–column joints, further investigation of this aspect is necessary.

Embedded beams

The performance of slab–column joints may be improved by applying various strengthening techniques, such as different forms of shear reinforcement, steel fibre, fibre-reinforced plastic, glass-fibre-reinforced plastic or the application of prestressed tendons. All these methods have been found to enhance the punching shear capacities and to improve the structural ductility of slab–column joints (Adetifa and Polak, 2005; Ebead and Marzouk, 2004; Ramos and Lucio, 2008). Another strengthening measure, that is, embedded beams, to be studied herein, is a seismic design requirement for building construction as specified in the Chinese design code GB 50011-2010 (MCPRC, 2010a). The effectiveness of such a strengthening technique has not been systematically studied. Therefore, it has become one of the key aspects to be examined in this study. Indeed, the arrangement of the embedded beams within the slab strip above the column has been proven capable of increasing the post-punching resistance and improving the ductility and integrity of the entire system, as observed in our tests (see section 'Strengthened specimens UPS-S1 and DPS-S1').

To sum up, the primary purpose of this work is to investigate the post-punching behaviour under UPS and DPS failure modes and the effectiveness of the strengthening technique, – that is, embedded beams. A series of experimental tests was conducted on four slab–column joint specimens (UPS and DPS, without embedded beams, and UPS-S1 and DPS-S1, with embedded beams) with appropriate slab in-plane restraint. Damage and failure modes of the specimens under large deformations were examined, to explore the post-punching mechanism of the specimens. A numerical simulation was also performed to evaluate the contributions of the concrete and reinforcement in resisting the collapse of the slab–column joints.

Experimental programme

Specimen design

Figure 2 provides a plan view of the prototype structure and test setup. The prototype structure is a three-storey 4×4 bay RC flat plate structure. A series of one-third scaled slab–column joint specimens with dimensions of $2000 \times 2000 \times 90$ mm, taken from the ground floor of the prototype structure, were cast and tested. The boundary of the joint is denoted by the line of contraflexure (Figure 2(a)). To better reflect the actual continuity of this boundary within the prototype structure, its periphery was designed by adding boundary beams, which provided anchorage to the slab reinforcement (Figure 3). The sectional dimensions of the boundary beams for all specimens were 300×380 mm. At the centre of each specimen, a concrete column stub with a 150×150 mm cross-section and 90 mm and 120 mm extrusions from the top surface and soffit of the slab, respectively, was built. For the UPS case considered in this study, the specimens were tested upside down under downward loading, which is similar to an existing experiment (Ruiz *et al.*, 2013). For the DPS case, the specimen was tested upright and was also subjected to downward loading. To achieve both DPS and UPS failure patterns using the downward loading device, the longitudinal reinforcements were arranged as follows. (*i*) For the DPS specimens, the flexural reinforcement (FR) and IR were arranged at the top and bottom of the slabs, respectively (Figure 3(c)). (*ii*) For the UPS specimens, the FR and IR bars were placed in reverse in the slabs (Figure 3(d)). Note that the IR bars in each UPS specimen were also bent down at the slab–boundary beam interface and further extended to the outer edge of the boundary beams (Figure 3(d)). In this way, the four edges of both the DPS and UPS specimens were subjected to negative bending moment through which the rotational restraint could be released at the onset of tensile cracks in the top concrete cover. Hence, the horizontal restraint and the rotational release along the contraflexure lines could be properly achieved, so that the in-plane tensile forces could be provided by the slab after the occurrence of punching shear failure.

Flat plate structures are widely constructed in Australia, and its relevant design standards are relatively mature. As such, the

layout of reinforcement was designed in accordance with the Australian building code AS3600 (SA, 2009). Conversely, the additional embedded beams for specimens DPS-S1 and UPS-S1 were designed based on the Chinese building code GB 50010-2010 (MCPRC, 2010b), owing to its seismic design considerations for structures. The Chinese code also has more specific detailing requirements for embedded beams. In general, both the Australian and Chinese design requirements were satisfied in the design of the prototype structure. Note that the reinforcement arrangement detailed in Figures 3 and 4 of the DPS and UPS specimens were identical to those of the prototype structure, regardless of their opposite punching directions.

Table 1 summarises the reinforcement details in the slabs for the four specimens. Longitudinal bars, of HRB400 grade, and stirrups, of HRB300 grade were provided for the specimens with embedded beams only. The boundary beams were reinforced with 12 mm diameter HRB400-grade longitudinal bars with a steel ratio of 1% and 8 mm dia. HRB300-grade

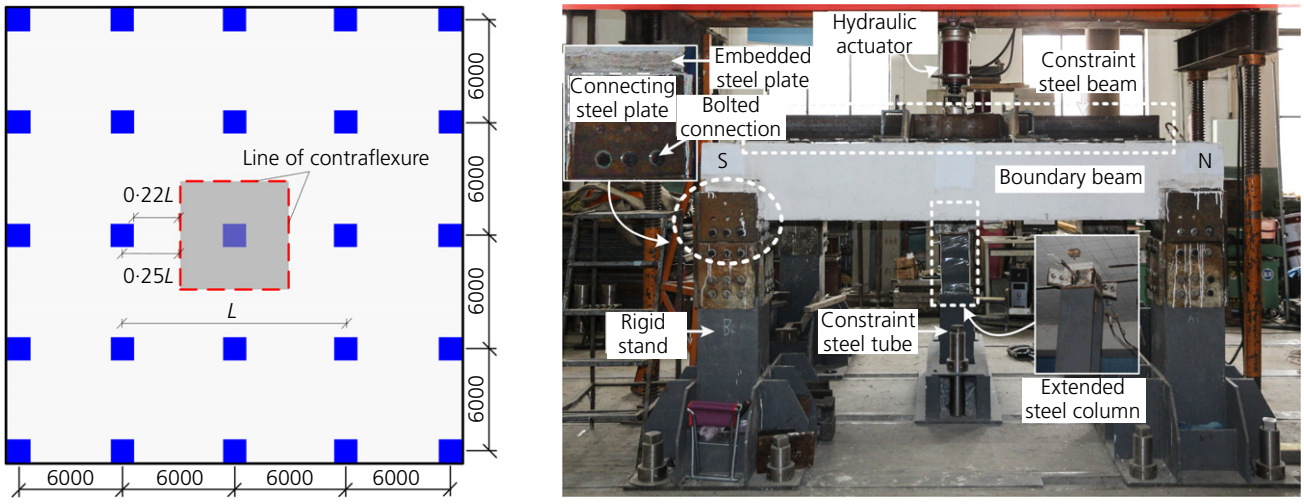

(a) (b)

Figure 2. Prototype structure and test setup: (a) plan view of prototype structure (dimensions in mm); (b) test setup

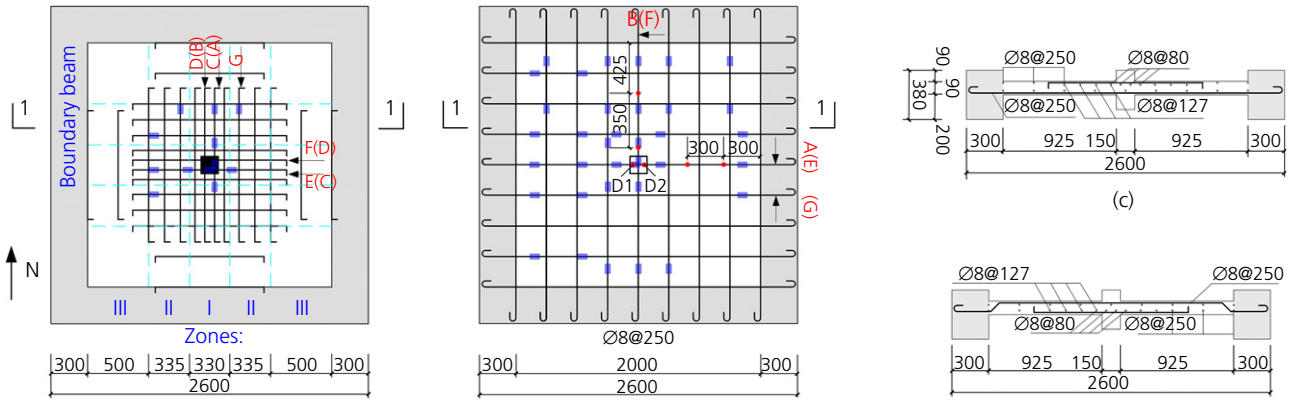

Note: D/C/G/F/E represent rebars in UPS-1; B/A/D/C in parentheses represent rebars in DPS-1

(a)

Note: B/A represent rebars in UPS-1; F/E/G in parentheses represent rebars in DPS-1

(b)

Figure 3. Reinforcement in DPS-1 and UPS-1: (a) FR; (b) IR; (c) DPS-1; (d) UPS-1 (dimensions in mm). ▬, steel strain gauge used in section 'Experimental observation and post-punching mechanisms'; ●, linear variable differential transformer. Details of reinforcement in Zones I to III are given in Table 1, where Zones I and II denote the column strip and Zone III represents the middle strip

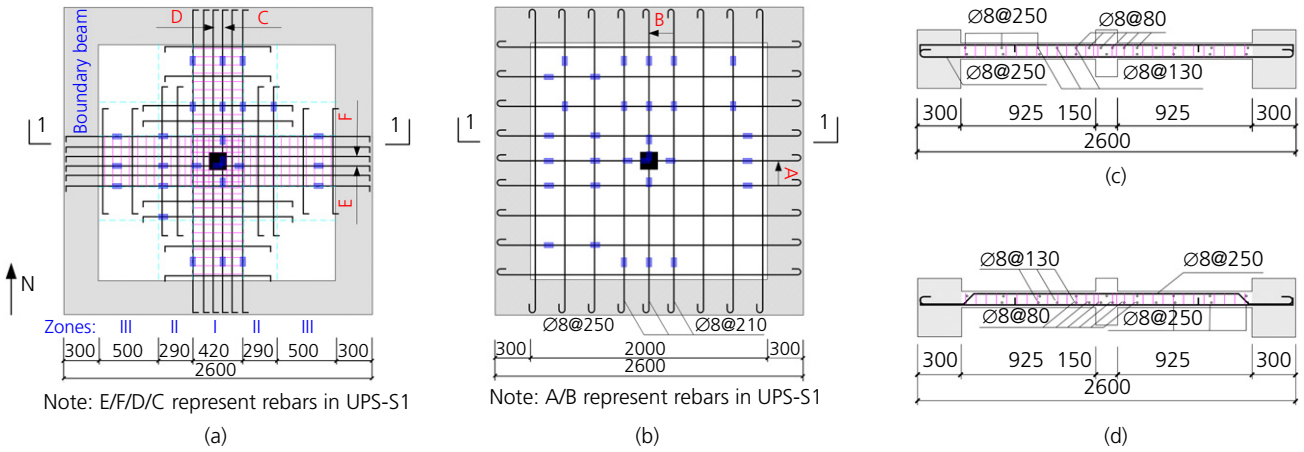

Figure 4. Reinforcement in DPS-S1 and UPS-S1: (a) FR; (b) IR; (c) DPS-S1; (d) UPS-S1 (dimensions in mm). ▬, steel strain gauge. Details of reinforcement in Zones I to III are given in Table 1, where Zones I and II denote the column strip and Zone III represents the middle strip

Table 1. Reinforcement details in slabs

Specimens	IR	FR			Stirrup
DPS-1/UPS-1	∅8@250[a]	Zone I ($d \le b + 2\ h$) ∅8@80[b]	Zone II ($d > b + 2\ h$) ∅8@127[b]	Zone III ∅8@250[c]	— —
DPS-S1/UPS-S1	Zone I/II ∅8@250/∅8@210[a]	Zone I ($d \le b + 2 \times 1{\cdot}5\ h$) ∅8@80[a]	Zone II ($d > b + 2 \times 1{\cdot}5\ h$) ∅8@130[b]	Zone III ∅8@250[c]	Zone I&II/III ∅4@50/∅4@70[d]

[a] $L_s = 2560$ mm, [b] $L_s = 1260$ mm, [c] $L_s = 890$ mm, [d] $L_s = 420$ mm

Table 2. Material properties

Type	Yield strength, f_y: MPa	Ultimate strength, f_u: MPa	Elastic modulus, E: GPa	Ratio of elongation, e: %	Cubic compressive strength of concrete, f_c: MPa
∅4	667	734		5	
∅8	298	471		29	
⌀8	436	643	205	24	31
⌀12	511	608		15	

stirrups. All the specimens were cast with C30-grade concrete. The material properties of the reinforcement and concrete are summarised in Table 2.

Test setup and instrumentation

In each specimen, a total of four pairs of steel plates were embedded on the side surfaces of the four corners of the boundary beams, to connect the specimen to four rigid stands through bolts and welding (Figure 2). The stands had sufficient rigidity and height, providing adequate fixity to the specimen and ample space to allow the specimen to undergo large deformations. Another four pairs of steel plates were also embedded at the top surface of each boundary beam, enabling connection with a hash-shaped steel beam, by which sufficient horizontal restraint was provided by the boundary beams and the steel beam. The experimental results showed that the horizontal displacements of the boundary beams were less than 2 mm (1/1000 of the span), confirming the effectiveness of inclusion of the boundary beams and the hash-shaped steel beam.

Referring to an existing slab–column joint test (Mirzaei and Muttoni, 2008), the quasistatic pushdown loading method was used and a downward displacement was applied to the top of the column stub just above the removed column. The lower part of the column stub was bolt-connected to a short steel column, which was then inserted into a steel tube fixed to the ground. In doing so, the column was allowed to move in the vertical direction only, and the other degrees of freedom,

including rotational and horizontal displacements of the stub, were fully restrained.

Experimental observation and post-punching mechanisms

The load–displacement curves shown in Figure 5 were recorded using two linear variable differential transformers located at the bottom column stub (D1 and D2 in Figure 3(b)). Clearly, for all the specimens, the load–displacement responses can be divided into three stages: a flexural stage, a punching shear failure stage and a suspension stage. Key points on the load–displacement curves are highlighted and represented by the load F (shown in Figure 5), and the corresponding displacement Δ. For DPS-1 and UPS-1 (Figure 5(a)), five key points can be identified, including the punching failure point (F_p, Δ_p), the load mechanism transition point (F_t, Δ_t) and three critical points in the suspension stage (F_{si}, Δ_{si}, $i = 1, 2, 3$), corresponding to the steel bars being either ruptured or pulled out. For DPS-S1 and UPS-S1 (Figure 5(b)), in addition to the points (F_p, Δ_p) and (F_t, Δ_t), another key point (F_s, Δ_s) represents the load stage corresponding to the rupture of all the rebars going through the column. The post-punching mechanisms (Figure 6) and the final damage modes (Figure 7) for each specimen are discussed next. Note that the reinforcing bars exhibiting critical phenomena are symbolised in Figures 3, 4 and 6.

Control specimen UPS-1

At a displacement of $\Delta = 36$ mm, punching shear failure occurred, leading to a sudden drop of the load from F_p to F_t (see Figure 5(a)). After that, the applied load was resisted by the four FR and two IR bars in two directions (see Figures 3(a) and 3(b)) through the column. At $\Delta = 101$ mm, one of the two IR bars ruptured (rebar A in Figures 3(b) and 6(a)) resulting in the second sudden drop of load F_{s1}. At this time, the angle of the punching crack could be clearly observed as approximately 45°. Further, one of the FR bars (rebar E) was totally detached from the slab soffit at $\Delta = 134$ mm, leading to a slight drop from load F_{s2}; following which no further increase of load was observed (Figure 5(a)). At $\Delta = 175$ mm, two FR bars (rebars C and D) ruptured simultaneously, causing the third sudden drop from load F_{s3}. Then another IR bar (rebar B) ruptured at $\Delta = 195$ mm. The loading process continued until $\Delta = 221$ mm. Finally, two FR bars going through the column and one FR bar in the vicinity of the column were all detached from the slab soffit (Figure 7(a)). All these critical displacement stages with the matching phenomena for UPS-1 are summarised in Table 3. The crack pattern of UPS-1 at the termination of the test is shown in Figure 8(a).

Control specimen DPS-1

As the punching direction of DPS-1 was reversed, this specimen exhibits different post-punching damage mechanisms as compared with UPS-1. (*i*) The order of reinforcement rupture has changed; two FR bars (rebars A and B in Figure 6(b)) ruptured first, followed by the rupture of one IR bar (rebar E). (*ii*) The concrete in the slab–column region (shaded in Figure 7(b)) was damaged in shear, at a displacement of $\Delta = 138$ mm. This is because more FR bars in the top of the slab than bottom IR bars generated larger shear forces to the concrete in this region. (*iii*) The IR bars were anchored into the boundary beams; hence, they were still effective in carrying the applied load even though they already partially pulled out of the concrete at the column region (see Figure 7(b)). The crack pattern of DPS-1 at the termination of the test is shown in Figures 8(c) and 8(d).

The post-punching stiffnesses of UPS-1 and DPS-1 under the first substage (from F_t to F_{s1} in Figure 5(a)) were much larger

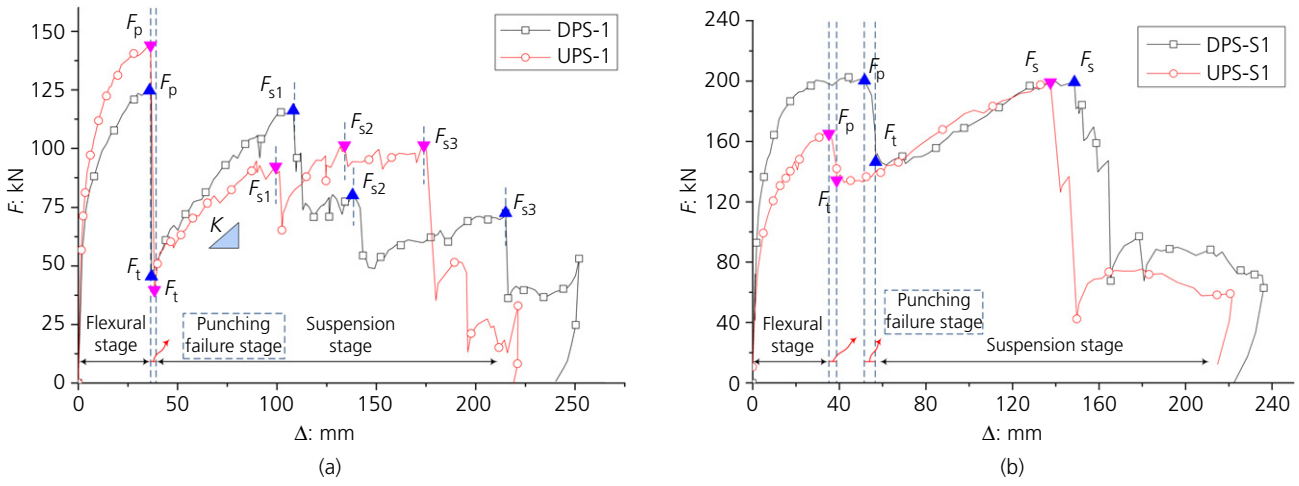

Figure 5. Load–displacement curves of four specimens: (a) DPS-1 and UPS-1; (b) DPS-S1 and UPS-S1

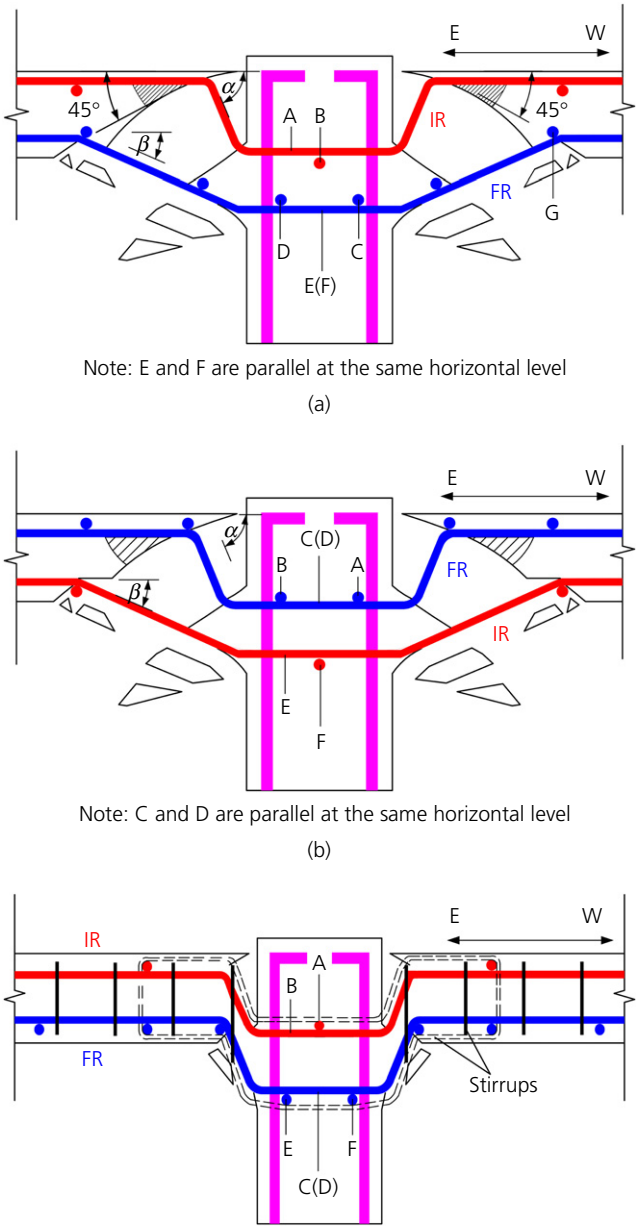

Figure 6. Post-punching mechanisms of three specimens: (a) UPS-1; (b) DPS-1; (c) UPS-S1. Shaded area denotes concrete support to reinforcement

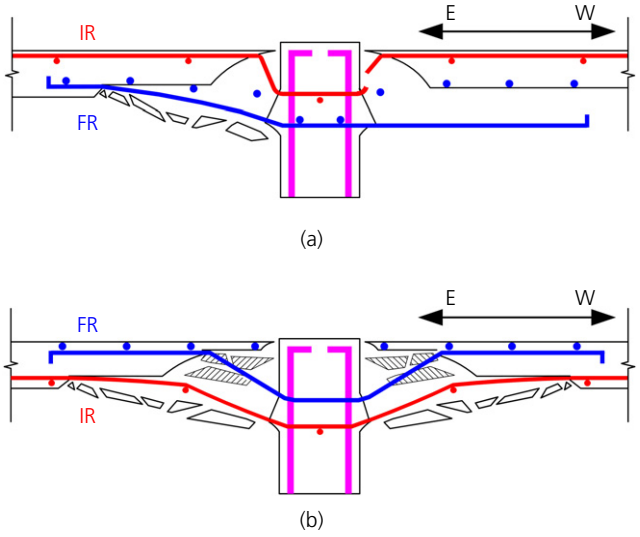

Figure 7. Final damage modes in UPS-1 and DPS-1: (a) UPS-1, FR bars pulled out and detached from slab soffit; (b) DPS-1, IR bars pulled out and concrete core damaged in shear

than those under the other two substages (F_{s1} to F_{s2} and F_{s2} to F_{s3}). Hence, the post-punching resistance under the first substage can be considered to make a major contribution to the collapse resistance. In the first substage, the bend-down angles of the top rebars in UPS-1 and DPS-1 ($\alpha \approx 86°$) were much greater than those of the bottom rebars ($\beta \approx 50°$). Because α is much greater than β, the strain and the vertical component of the axial force in the top reinforcement were much greater than those in the bottom reinforcement. This implies that the bearing capacity in this stage was predominantly contributed by the top reinforcement in the column region. Note that in DPS-1, four (A, B, C, D) and two (E, F) rebars were located in the top and bottom of the slab, respectively (Figure 6(b)), and these rebars were inversely positioned in UPS-1 (Figure 6(a)). Therefore, DPS-1 was able to develop a 15% higher stiffness, K, at this stage, as can be seen from the load–displacement curves shown in Figure 5(a), than that developed by UPS-1 at the beginning of this stage. Furthermore, owing to the larger K in DPS-1, the load-carrying capacity F_{s1} in DPS-1 ($F_{s1} = 116$ kN) was 22% higher than that in UPS-1 ($F_{s1} = 95$ kN) (Figure 5(a)).

Strengthened specimens UPS-S1 and DPS-S1

Compared with UPS-1, the specimen strengthened with the embedded beams (UPS-S1) demonstrates the following differences in the damage mode. (*i*) More slab reinforcement within the embedded beams, but not going through the column, participated in resisting the applied load. Hence, the crack distribution was more uniform, and the cracks were widened. (*ii*) The stirrups provided in the embedded beams enabled the longitudinal bars going through the column region to develop similar levels of strain, which delayed the rupture of the IR bar (rebar A in Figure 6(c)), as shown in Figures 5(a) and 5(b) ($\Delta_{s1} = 101$ mm for UPS-1, $\Delta_s = 138$ mm for UPS-S1). This is followed by the longitudinal bars going through the column rupturing sequentially with a very small increase in deformation. (*iii*) Since the integrity of the specimen with embedded beams was improved, although a small amount of the concrete cover for FR bars was damaged, these bars were still able to work together with the concrete within the punching area, as shown in Figure 6(c). All the rebars going through the column

Table 3. Vertical joint displacements with matching phenomena

Typical phenomenon	UPS-1: mm	DPS-1: mm	UPS-S1: mm	DPS-S1: mm
Flexural cracks at bottom of slabs	9	6	4	4
Punching failure (Δ_p)	36	36	35	45
Mechanism transition point (Δ_t)	37	37	42	57
Initial rupture of IR rebar	101 (Δ_{s1})	215 (Δ_{s3})	138 (Δ_s)	165
Detachment of FR rebar from slab soffit	134 (Δ_{s2})	—	—	—
Shear failure of concrete core	—	138 (Δ_{s2})	—	—
Initial rupture of FR rebar	175 (Δ_{s3})	108 (Δ_{s1})	147	148 (Δ_s)
Second rupture of FR rebar	175 (Δ_{s3})	113 (Δ_{s1})	147	152
Second rupture of IR rebar	195	—	138 (Δ_s)	165
Rupture of all rebars going through the column stub	—	—	147	165
End of test	221	252	221	225

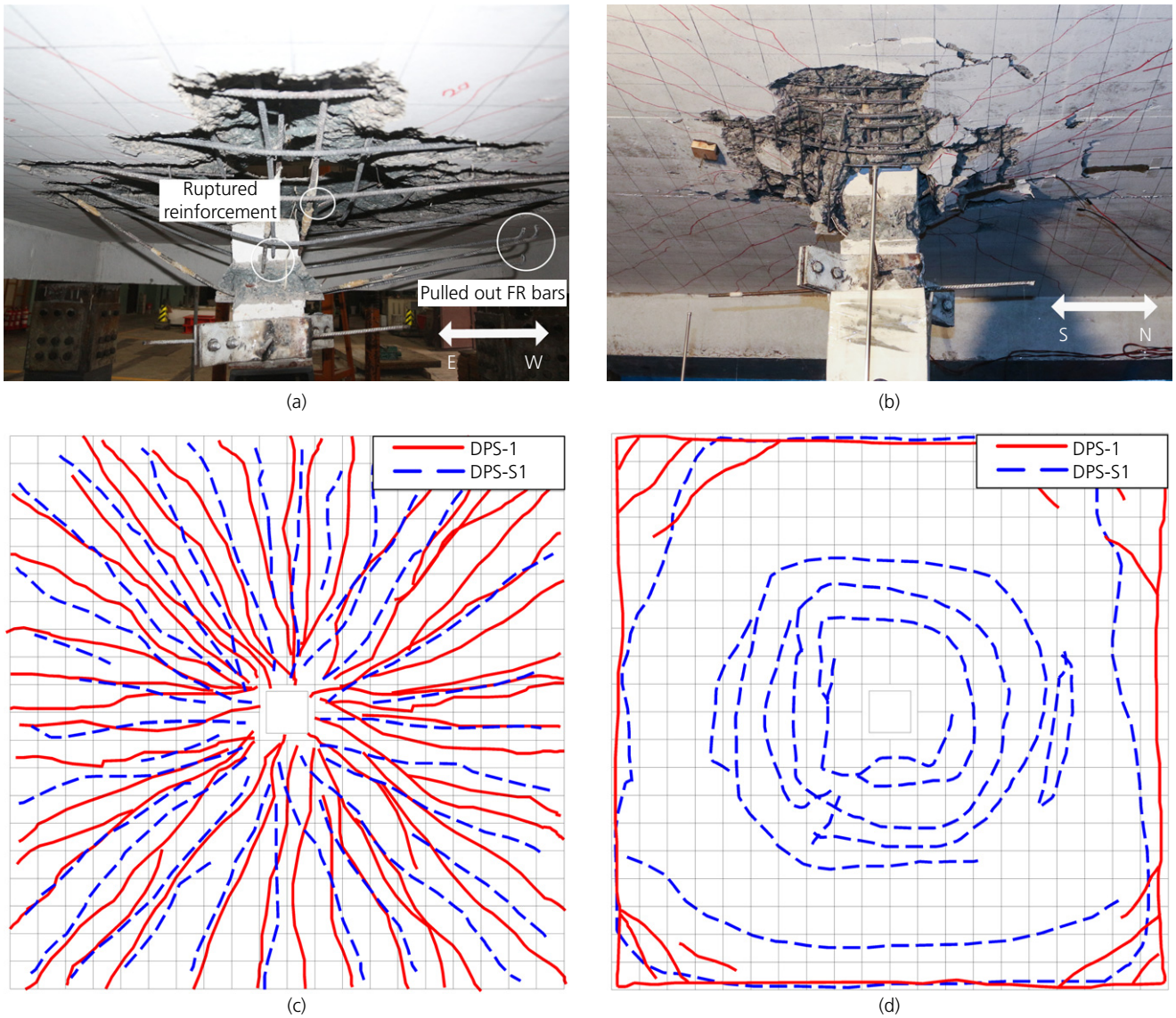

(a) (b) (c) (d)

Figure 8. Crack patterns of the specimens: (a) bottom view of UPS-1; (b) bottom view of UPS-S1; (c) bottom surface cracks of DPS-1/DPS-S1; (d) top surface cracks of DPS-1/DPS-S1

ruptured at $\Delta_s = 150$ mm as shown in Figure 5(b). The crack pattern of UPS-S1 at the termination of the test is shown in Figure 8(b). The final damage mode of DPS-S1 was very similar to that of UPS-S1 (Figure 6(c)). Figures 8(c) and 8(d) compare the final crack patterns of DPS-1 and DPS-S1 on their bottom and top surfaces, from which DPS-S1 demonstrates more uniformly distributed cracks than DPS-1, particularly on the top surface.

Compared with the control specimens (UPS-1 and DPS-1), the differences in the failure mechanisms of UPS-S1 and DPS-S1 can be identified. (*i*) The post-punching mechanisms of the specimens with embedded beams were identical, regardless of their opposite punching directions. (*ii*) The specimens with embedded beams exhibited increased resistant capacities under both the flexural and suspension mechanisms. The inclusion of stirrups within the embedded beams improved the ductility and load-carrying capacity of UPS-S1, reflected by a 37% increase in Δ_{s1} (UPS-S1: $\Delta_s = 138$ mm; UPS-1: $\Delta_{s1} = 101$ mm) and a 97% increase in F_s (UPS-S1: $F_s = 188$ kN; UPS-1: $F_{s1} = 95$ kN), respectively. The stirrups in the embedded beams also improved the ductility and load-carrying capacity of DPS-S1, reflected by a 37% increase in Δ_{s1} (DPS-S1: $\Delta_s = 148$ mm; DPS-1: $\Delta_{s1} = 108$ mm) and a 72% increase in F_s (DPS-S1: $F_s = 200$ kN, DPS-1: $F_{s1} = 116$ kN), respectively.

The strain development of the rebars going through the column for UPS-S1 and DPS-S1 was much more similar compared with the large variations of the strain development between UPS-1 and DPS-1. This is because the stirrups within the embedded beams provided effective in-plane restraints to the longitudinal bars going through the column (rebars A–F in Figure 6(c)). For instance, it is evident in Figure 9 that the strain development in top and bottom reinforcement (i.e. rebars B and C) in UPS-S1 was similar in comparison with that in UPS-1. This was also the case for DPS-S1. As a result, all the through-column rebars in both UPS-S1 and DPS-S1 ruptured in succession within a small range of displacement growth. Note that the bearing capacity of UPS-S1 under the flexural mechanism was lower than that in DPS-S1. This is because in DPS-S1, the top FR bars within zone I (Figure 4(a)) were extended into the boundary beams instead of being bent down to the bottom of the slab, thereby resulting in an increase in F_p and Δ_p.

Numerical analysis

To fully understand the post-punching mechanisms of the slab–column joints, three-dimensional (3D) finite-element models were built in accordance with the experimental specimens using the explicit finite-element software LS-DYNA (LSTC, 2015).

Modelling details and verification

In the numerical model, concrete was simulated using eight-node 3D solid Lagrangian elements; the continuous surface cap model MAT_159 was employed to simulate the behaviour of the concrete material. Reinforcing bars were explicitly modelled as two-node Hughes–Liu beam elements with 2×2 Gauss quadrature integration. For the steel material, an isotropic elastic–plastic material model, namely the Mat Piecewise Linear Plasticity model (MAT_024), was used. Different mesh sizes were adopted for the solid elements simulating the column and the concrete slab. Specifically, a 15 mm mesh size was used for the column and critical punching regions in the slab, and 15·5 mm for the remaining slab regions. Two mesh sizes of 18 mm and 20 mm were used for rebar elements. In addition, the element erosion function for the concrete was also considered, to model the spalling and separation of concrete under high tensile forces. In this study, the criteria for erosion of concrete and reinforcement elements were based on

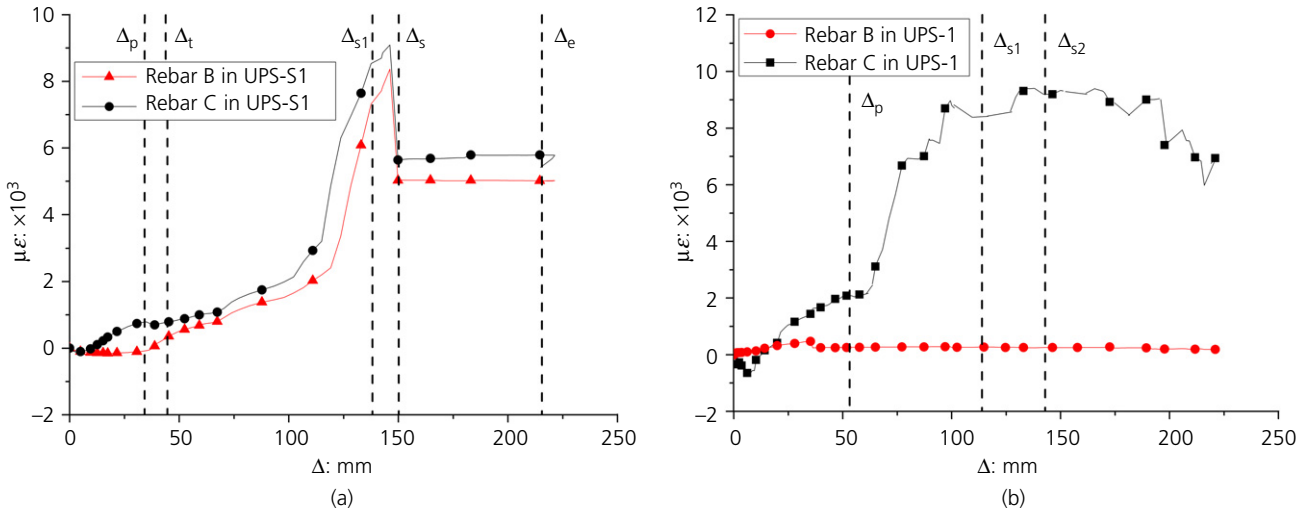

Figure 9. Comparison of slab reinforcement strains in: (a) UPS-S1 and (b) UPS-1

the maximum effective strain of concrete and the maximum effective plastic strain of steel, respectively. The erosion values set in the models were calibrated against the test specimens. By virtue of symmetry with respect to the geometric, loading and boundary conditions, only a quarter model of each slab–column joint specimen was simulated.

Figure 10 compares the load–displacement curves between the test and numerical results for the two pairs of specimens (DPS-1 and UPS-1, DPS-S1 and UPS-S1), which are in good agreement. However, in all four models, the use of the element erosion function for concrete resulted in a large amount of deletion of concrete elements, in turn causing a slightly larger reduction in the shear capacity at the onset of punching shear failure. In the real experimental tests, however, after the occurrence of punching shear failure, damaged concrete in the critical punching region was still able to transfer loads and function as an anchorage for reinforcing bars. The punching and post-punching shear capacities, denoted V_p and V_{pp}, respectively, which are the peak F values in the flexural and post-punching stages (Figure 10), are summarised in Table 4. $V_{p,e}$ and $V_{pp,e}$ represent the test results, and $V_{p,s}$ and $V_{pp,s}$ represent the numerical results. Comparing DPS-1 and UPS-1, the maximum numerical values of $V_{p,s}$ and the corresponding vertical displacements of the test and numerical results are fairly similar. Conversely, the numerical values of $V_{pp,s}$ at the suspension stage are 16% and 25% larger than those of the tests ($V_{pp,e}$), for DPS-1 and UPS-1, respectively. This is because the concrete–steel bond–slip relationship was not taken into consideration in the models; this resulted in a stronger bond between the concrete and reinforcing bars, hence larger values of $V_{pp,s}$. For DPS-S1 and UPS-S1, the differences between the test and numerical results are greater than those in DPS-1 and UPS-1, 4% and 23% in V_p and V_{pp}, respectively, for DPS-S1, and 3% and 11%, respectively, for UPS-S1. In particular, the large discrepancies in V_{pp} are attributable to the fact that the IR bars in the strengthened specimens DPS-S1/UPS-S1 were more effective in transferring the load in the tests; whereas the integrity bars were less effective, owing to the deletion of the concrete elements in the numerical analysis, as described. In other words, the contribution of concrete confinement to the integrity bars (further evidence is provided in the next section) was neglected in the models, in that the concrete in the critical punching region was mostly deleted after reaching its shear strain criterion. This also explains the more significant reductions in the numerical shear

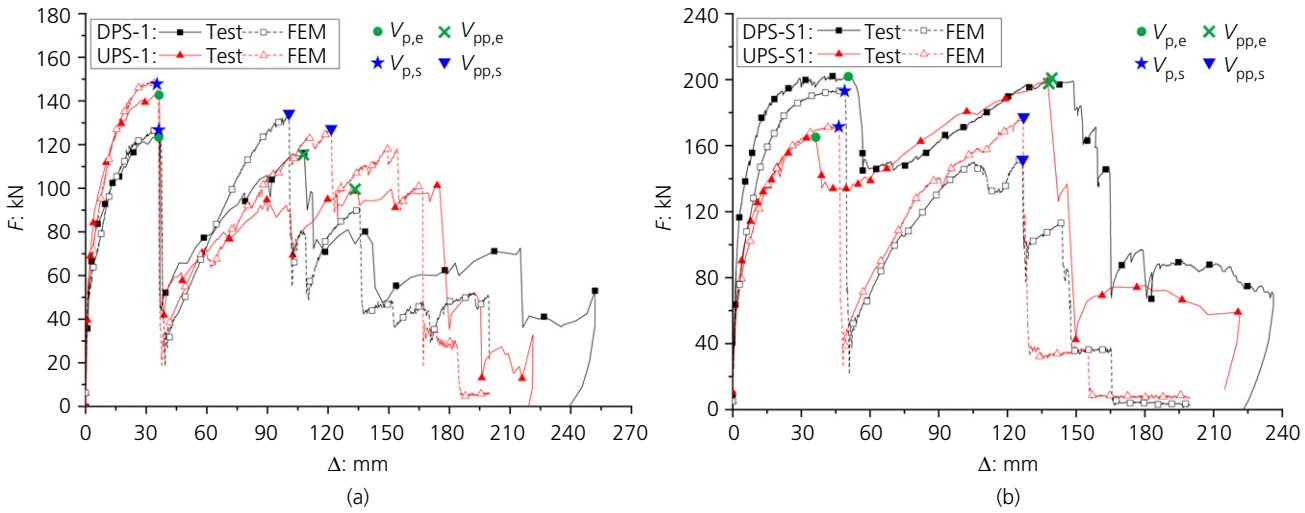

Figure 10. Comparisons of experimental and numerical load-deflection curves: (a) DPS-1 and UPS-1; (b) DPS-S1 and UPS-S1. FEM, finite-element modelling

Table 4. Comparison of punching and post-punching shear capacities

	Experiment		Simulation			
Specimen	$V_{p,e}$: kN	$V_{pp,e}$: kN	$V_{p,s}$: kN	$V_{pp,s}$: kN	$V_{p,s}/V_{p,e}$	$V_{pp,s}/V_{pp,e}$
DPS-1	124	116	128	135	1·032	1·164
UPS-1	144	102	148	128	1·028	1·255
DPS-S1	201	198	193	153	0·960	0·773
UPS-S1	165	199	170	177	1·030	0·889
Mean					1·010	1·020
Coefficient of variance					0·040	0·220

capacities and lower values of $V_{pp,s}$ in the post-punching stage for both DPS-S1 and UPS-S1. Nevertheless, as shown in Table 4, the mean and coefficient of variance of simulated-to-experiment $V_{p,s}/V_{p,e}$ (1·01 and 0·04, respectively) and $V_{pp,s}/V_{pp,e}$ (1·02 and 0·22, respectively) confirm that the proposed modelling techniques are able to satisfactorily predict both the punching and post-punching shear capacities recorded in the experiments.

Contributions of concrete and through-column reinforcing bars to overall load capacity

Based on the numerical analysis results, Figure 11 presents the contribution of the concrete within the punching shear area (PSA) and that of the six through-column reinforcing bars to the overall load capacity for all the four specimens. Note that the PSA is defined as the square region of 45×45 mm bounded by half of the slab effective depth away from each column face, according to the provisions of ACI 318-11 (ACI, 2011).

The curves with square markers in Figure 11 represent the concrete contribution to the overall load capacity within the PSA and the curves with triangle markers represent the contribution from the vertical component of the load transferred to the six through-column reinforcements. Before punching shear failure occurred, the two materials, concrete and reinforcement, within the PSA, worked well together. It can be seen from the numerical load–displacement curves, presented in Figure 11, that the concrete within the PSA contributed about half of the load capacity in all specimens, whereas the contribution of the six through-column reinforcements is smaller than 10% for all the specimens. After punching shear failure takes place, the concrete within the PSA makes almost no contribution to the load-bearing capacity but only acts as an anchorage to the slab reinforcement. Note that in UPS-1 and DPS-1, the

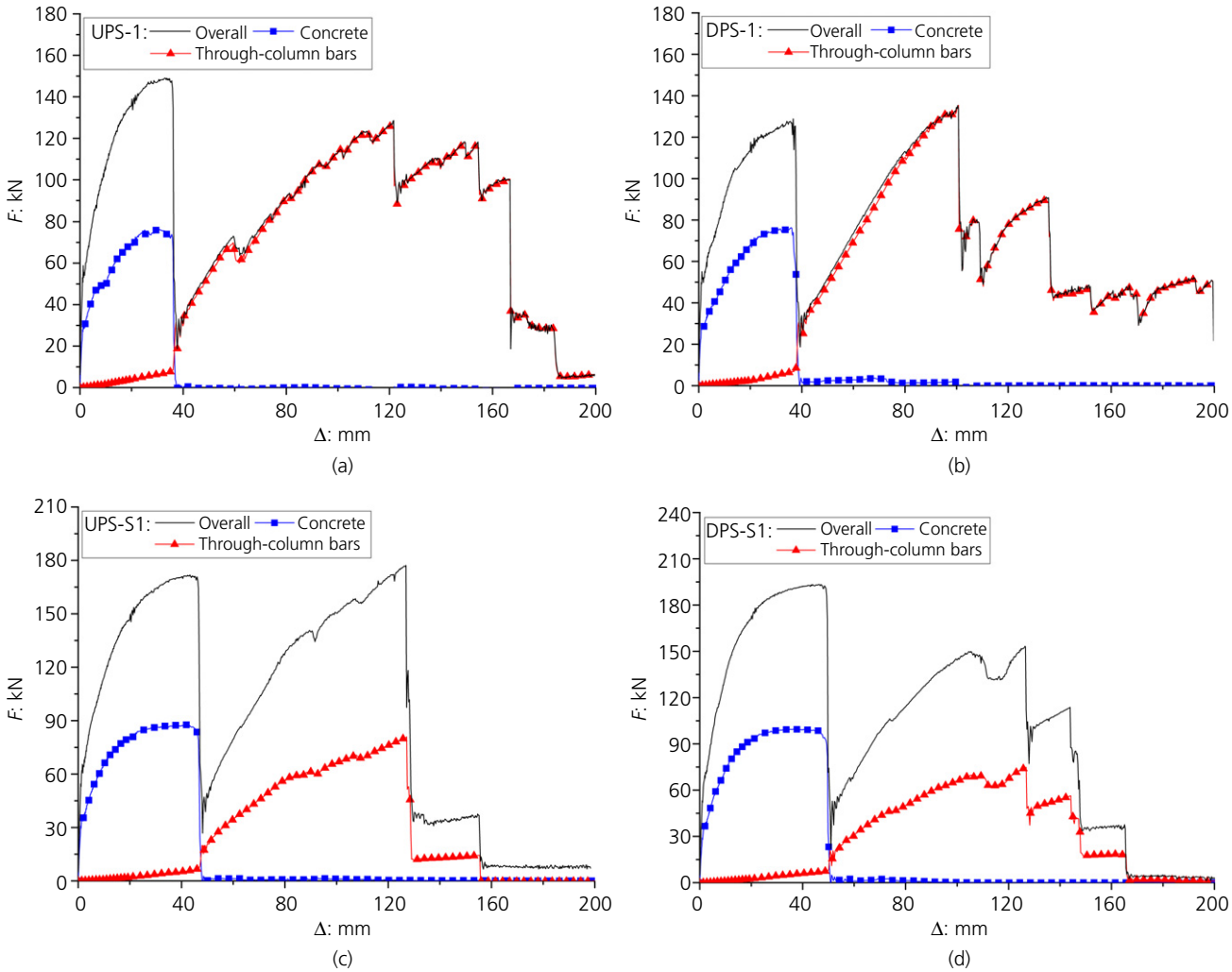

Figure 11. Contributions of concrete within punching shear area and through-column reinforcing bars to overall load capacity: (a) UPS-1; (b) DPS-1; (c) UPS-S1; (d) DPS-S1

through-column reinforcing bars provide most of the resistance (more than 99%) in the post-punching stage. This is indicated by the curves with triangle markers in Figures 11(a) and 11(b), which almost match exactly with the black curve representing the overall load capacity. For UPS-S1 and DPS-S1 (Figures 11 (c) and 11(d)), however, owing to the improved structural integrity in the form of confining action provided by the stirrups, all the reinforcing bars within the embedded beams contribute to the overall load capacity. Therefore, the contribution from the six through-column bars is reduced to about 50% of the total load capacity.

Conclusions

This paper reports on an experimental and numerical investigation of the mechanical performance of four RC flat slab–column joint specimens under different punching directions, with and without embedded beams. The post-punching behaviour and the resistant capacity against progressive collapse are highlighted with detailed discussions. The following conclusions are drawn from the test and simulation results.

- After punching shear failure occurred, the post-punching bearing and deformation capacities of the slab–column joints were dominantly determined by reinforcement going through the column and reinforcement confined by the stirrups; this was also the case for joints with embedded beams. The specimens almost lost all their bearing capacities when all the through-column reinforcement ruptured.
- The failure mechanisms in UPS-1 and DPS-1 were different. In the punching failure stage, DPS-1 was found to exhibit 16% smaller punching shear capacity compared with that of UPS-1, owing to the steel bars rupturing in a reversed order. In the suspension stage, UPS-1 reached its peak resistance when one of the IR bars ruptured and one of the FR bars detached from the concrete from the slab soffit. The peak resistance in DPS-1 was reached when one of the FR bars ruptured, whereas the IR bars remained intact, and the peak capacity was 22% higher than that of UPS-1, owing to the inverted layout of the reinforcement.
- The post-punching mechanisms of UPS-S1 and DPS-S1 were almost identical, regardless of their opposite punching directions, owing to the restraints provided by the stirrups in the embedded beams. Moreover, the addition of the embedded beams facilitated greater deformation and load capacities in the suspension stage, causing the corresponding displacement to be delayed by 37% in both UPS-S1 and DPS-S1, and the punching shear resistance to be increased by 97% and 72% in UPS-S1 and DPS-S1, respectively, compared with those in UPS-1 and DPS-1.
- It was found in the numerical study that the through-column reinforcing bars in the slab contributed more than 99% of the post-punching resistance in the specimens without embedded beams. For the specimens with embedded beams, the stirrup confinement to the reinforcement within the column strip helped to improve the integrity and ductility of the slab and alter the failure mode of the slab–column joints. The contribution from the six through-column bars was reduced to 50% of the total load capacity because more bars contributed to the overall load resistance.

Acknowledgements

The authors are grateful for financial support received from the National Natural Science Foundation of China (grant number 51578018), the National Key Research and Development Program of China (grant number 2016YFC0701400), the Beijing Nova Program (grant number xx2017093), the Australian Research Council through an ARC Discovery Project (grant number DP150100606) and the International Research Cooperation Seed Fund of Beijing University of Technology (grant number A04).

REFERENCES

ACI (American Concrete Institute) (2011) ACI 318-11: Building code requirements for structural concrete and commentary. American Concrete Institute, Farmington Hills, MI, USA.

Adetifa B and Polak MA (2005) Retrofit of slab column interior connections using shear bolts. *ACI Structural Journal* **102(2)**: 268–274.

ASCE (American Society of Civil Engineers) (2010) ASCE 7-10: Minimum design loads for buildings and other structures. ASCE, Reston, VA, USA.

Carvalho AL, Melo GS, Gomes RB and Regan PE (2011) Punching shear in post-tensioned flat slabs with stud rail shear reinforcement. *ACI Structural Journal* **108(5)**: 523–531.

Criswell ME (1974) *Static and Dynamic Response of Reinforced Concrete Slab-Column Connections*. ACI Special Publication 42-31721-746. American Concrete Institute, Farmington Hills, MI, USA.

Dusenberry DO (2010) *Handbook for Blast-Resistant Design of Buildings*. John Wiley & Sons, Inc., Hoboken, NJ, USA.

Ebead U and Marzouk H (2004) Fiber-reinforced polymer strengthening of two-way slabs. *ACI Structural Journal* **101(5)**: 650–659.

Elstner RC and Hognestad E (1956) Shearing strength of reinforced concrete slabs. *ACI Journal Proceedings* **53(1)**: 29–58.

Gardner NJ, Huh J and Chung L (2002) Lessons from the Sampoong department store collapse. *Cement Concrete Composites* **24(6)**: 523–529.

Guandalini S, Burdet OL and Muttoni A (2009) Punching tests of slabs with low reinforcement ratios. *ACI Structural Journal* **106(1)**: 87–95.

Habibi F, Redl E, Egberts M, Cook WD and Mitchell D (2012) Assessment of CSA A23.3 structural integrity requirements for two-way slabs. *Canadian Journal of Civil Engineering* **39(12)**: 351–361.

Hawkins NM and Mitchell D (1979) Progressive collapse of flat plate structures. *ACI Structural Journal* **76(7)**: 775–808.

Keyvani L, Sasani M and Mirzaei Y (2014) Compressive membrane action in progressive collapse resistance of RC flat plates. *Engineering Structures* **59**: 554–564.

Liu JR (2014) *Progressive Collapse Analysis of Older Reinforced Concrete Flat Plate Buildings Using Macro Model*. PhD thesis, University of Nevada, Las Vegas, NV, USA.

LSTC (Livermore Software Technology Corporation) (2015) *LS-DYNA Keyword User's Manual*. Livermore Software Technology Corporation, Livermore, CA, USA.

McPeake FA (1980) *Post-punching Resistance of Internal Slab-Column Connection*. BSc honours project. Department of Civil Engineering, Queen's University of Belfast, Belfast, UK.

MCPRC (Ministry of Culture of the People's Republic of China) (2010a) GB50011-2010: Code for seismic design of buildings. Ministry of Housing and Urban Rural Development of the People's Republic of China, Beijing, China.

MCPRC (2010b) GB50010-2010: Code for design of concrete structures. Ministry of Housing and Urban Rural Development of the People's Republic of China, Beijing, China.

Melo GSSA and Regan PE (1998) Post-punching resistance of connections between flat slabs and interior columns. *Magazine of Concrete Research* **50(4)**: 319–327.

Mirzaei Y (2010) *Post-punching Behavior of Reinforced Concrete Slabs*. PhD thesis, EPFL, Lausanne, Switzerland.

Mirzaei Y and Muttoni A (2008) *Tests of the Post Punching Behavior of the Reinforced Concrete Flat Slabs*. IS-Béton, Lausanne, Switzerland.

Mitchell D and Cook WD (1984) Preventing progressive collapse of slab structures. *Journal of Structural Engineering* **110(7)**: 1513–1532.

Peng ZH, Orton SL, Liu JR and Tian Y (2017) Effects of in-plane restraint on progression of collapse in flat-plate structures. *Journal of Performance of Constructed Facilities* **31(3)**: 04016112.

Ramos AP and Lucio VJG (2008) Post-punching behavior of prestressed concrete flat slabs. *Magazine of Concrete Research* **60(4)**: 245–251.

Robertson IN, Riggs HR, Yim SCS and Young YC (2007) Lessons from hurricane Katrina storm surge on bridges and buildings. *Journal of Waterway Port Coastal and Ocean Engineering* **133(6)**: 463–483.

Ruiz MF, Muttoni A and Kunz J (2010) Strengthening of flat slabs against punching shear using post-installed shear reinforcement. *ACI Structural Journal* **107(4)**: 434–442.

Ruiz MF, Mirzaei Y and Muttoni A (2013) Post-punching behaviour of flat slabs. *ACI Structural Journal* **110(5)**: 801–811.

SA (Standards Australia) (2009) AS3600: Australian standard concrete structures. Standards Australia Limited, Sidney, NSW, Australia.

Wood JGM (2003) Pipers row car park collapse: identifying risk. *Concrete* **37(10)**: 29–31.

How can you contribute?

To discuss this paper, please submit up to 500 words to the editor at journals@ice.org.uk. Your contribution will be forwarded to the author(s) for a reply and, if considered appropriate by the editorial board, it will be published as a discussion in a future issue of the journal.